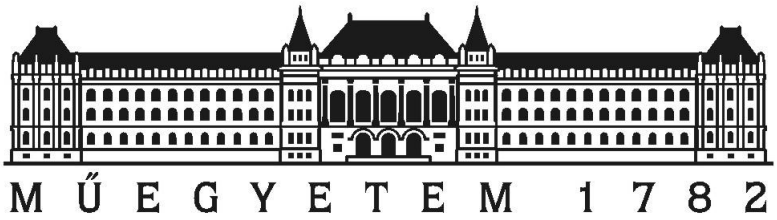

George Olah Doctoral School

Faculty of Chemical Technology and Biotechnology

Budapest University of Technology and Economics

FABRICATION AND MAGNETO-OPTICAL CHARACTERIZATION OF SILICON CARBIDE NANOPARTICLES TOWARDS BIOLABELING

Ph.D. Thesis

Author: Gyula Károlyházy

Supervisor: Ádám Gali

Consultant: János Madarász

Wigner Research Centre for Physics

2021

1. INTRODUCTION

One of the most actual challenges in the field of biochemistry/pharmacology is to be able to identify the processes in a biological system including the human body. To this end, these processes should be observed. This challenge leads us directly into the world of bioimaging, where the applied methods differ in complexity, sensitivity and required time as well. Generally they provide supplementary information to each other thus are usually used together.[1] The fluorescence based imaging techniques have many advantages like good resolution great sensitivity and simplicity. On the other hand it is quite hard to achieve proper biomarker. Biomarkers need to meet multiple criteria. They should be non-toxic and bioinert, appropiate for clearence (for that their diameter should be below 5.5 nm) and photostable.[2,3] Quantum dots have several advantages over dye probes.[4,5] First, quantum confinement makes it possible to tune their properties. They have higher quantum yield and are stable for long time during the aquisition. On the other hand they are barely soluble in aqueous systems. In addition many of them (e.g. CdSe nanocrystals) consists of hazardous toxic elements. To increase the solubility and the chemical stability usually additional modifications are applied to their surface which leads to larger particles.[6]

At the Wigner Research Centre for Physics as part of the Solid State Physics Department our research group has been working on a new *in vivo* biomarker based on silicon carbide which could fulfill all the related criteria. I joined this research in 2013 under the supervision of Ádám Gali. The motivation was to develop a fluorescent probe that is not just bright but has very good biocompatibility; therefore, it can be used for *in vivo* bioimaging, medical diagnostic, and even for therapy beyond the limitation of current alternatives.

Bulk SiC is a wide bandgap semiconductor which has excellent chemical and mechanical stability therefore it is good candidate for bioimaging. The only significant disadvantage of SiC is its luminescence because bulk SiC is emitting around 500-600 nm and that requires ultraviolet (UV) light for excitation. This is not appropriate for biological systems because photons with this energy could damage cells. For *in vivo* applications the optimal excitation and emittance should be between 700 and 1300 nm as the natural cell absorbtion in this range is low.[7,8]

There are more possible ways to modify the materials luminescence properties like doping the bulk SiC or irradiating it with various fluents. The aim of my work was to improve the fluorescence properties of SiC in order make it adequate for bioimaging.

2. THEORETICAL BACKGROUND

History and synthesis of Silicon Carbide

Silicon carbide in its natural form has been known to mankind only for the last 130 years. It barely occurs on our planet and was only discovered by Henri Moissan in 1893 in a meteorite. Honoring his name the mineral which contains SiC has been named moissanite. Due to its chemical and mechanical stability and outstandingly good resistance to harsh environment silicon carbide is a common form of stardust around carbon-rich stars thus originates from outside the solar system.

The sintering of SiC powders for bulk fabrication of high density ceramics is very difficult due to the covalent bonding which inhibits vacancy diffusion and with it the sintering itself. Additives and the use of high temperatures may be employed to aid the sintering process.

Silicon carbide shows polytypism which is a special case of polymorphism. Polymorphism is similar to allotropy and means that a solid material shows multiple crystal forms with identical molecular formula. More than 200 SiC polymorphs have been found by 1993 and additional 50 by 2008.[9] The stardust-SiC contains mostly cubic SiC (β-SiC).

Combustion synthesis (CS) is an effective technique to produce a wide variety of advanced materials that include powders and net shape products of ceramics, intermetallics, composites and functionally graded materials. The CS method has several advantages over traditional powder metallurgical technologies. These advantages include short synthesis time (eventually meaning minutes); ability to produce high purity products, since the extremely high-temperature conditions, which take place in the combustion wave, burn off most of the impurities. This approach also offers the possibilities for nanomaterials production.

The additional steps throughout the reactions which aim to remove the unreacted silicon and carbon are all strong oxidizing steps therefore the surface of the remaining bulk material is also oxidized and it determines the default surface of the obtained nanoparticles (NPs) as well which tends to be carboxyl terminated and in aqueous solutions shows a weak acidic character.

Defects and impurities in SiC

The electrical and optical properties of SiC heavily depend on the type of extrinsic and intrinsic defects. These defects have been intensively investigated in the past decades in SiC. The literature is quite voluminous about the properties of intrinsic point defects, vacancies, substitutions, interstitial defects, stacking faults and micropipes.

For creating defects one can use various type of irradiations or doping. In fact defects in SiC are often produced by high-energy particle bombardment. If the energy of these particles is high enough, the atoms in the lattice can actually be kicked out of their places. The primary defects created in this way are generally vacancies and interstitials, but in a binary compound like SiC also the antisites can be formed.[10,11]

The polytypism is not only important for the sole reason of understanding the single unit cell but also because it can “multiply” certain defects. Because of the polytypism the same defect can take several places in the crystal. The immediate vicinity of an intrinsic defect on either site is the same, but the second-nearest neighbors to the sites are different, which creates slightly different energy states in each case.

Surface chemistry and protein labeling

The oxidized surface of the as prepared NPs contains organic functional groups such as carboxyl and hydroxyl, stabilizing the nanoparticles in polar solvents, including biologically relevant media, without the need for surfactants or capping layers. Bonding with amino acids and could potentially open up the door for a SiC-based solid phase peptide synthesis, (SPPS) a concept that was introduced at 1963.[12] SPPS is based on attaching the first amino acid to a resin, then proceeding with peptide chain elongation to ultimately provide the target peptide.

Nanoparticles also show affiliation towards absorbing certain proteins on their surface, which often manifests in protein corona (PC) formation. As the cell detects corona coated NPs, the protein corona can dictate biological response to NPs. More importantly, an interaction like this

could potentially change the optical properties of the NPs.[13] It is worth noting that the typical NPs applied to *in vivo* systems are usually larger than 30 nm [14]
Regarding this topic the size of the NPs is the most important property as even the large proteins are usually smaller than 100 nm. Smaller NPs may be comparable in size with the proteins or even much smaller than them, and this generally defines the way these two objects interact with each other. If the sizes of the nanoparticle and the protein are comparable then they will interact like two proteins or like two nanoparticles. For very small nanoparticles and large proteins, we can predict a specific interaction where a nanoparticle can interact with a specific surface epitope or binding pocket of a protein.

Research objectives

Silicon carbide has excellent properties making SiC NPs a promising candidate for biological and optical application. However, the synthesis methods and certain impurities have strong influence on the optical properties of the product which are crucial for bioimaging and thus understanding of these methods needs to be improved to gain higher level of control over the obtained bulk material or nanoparticles. For *in vivo* application, the blue-green emission should be shifted to red, that might be achieved by introducing appropriate point defects. Before that, the effect of the bulk crystalline structure on the luminescence versus that of the surface states needs to be excessively studied. Eventually the material is intended for *in vivo* applications therefore its interaction with proteins are interesting.
Based on these needs I setup the following scientific goals and the direction of research:

1. The synthesis of SiC NPs should be understood in depth in order to gain control over the bulk materials properties and the size distribution of the NPs.

2. The role that the surface plays in the luminescence of NPs should be examined and answered.

3. The SiC NPs with approximate size of 5 nm-s should be suitable for in vivo applications and therefore functionalization should be attempted. Similarly, the interaction with a protein should be examined.

3. MATERIALS AND METHODS

SiC powder synthesis SiC synthesis was carried out in an induction furnace. The induction generator operates at 300 kHz and the anodic current at the peak performance is 3.5 A. The graphite crucible is 40 mm wide and 70 mm high, the wall thickness is 5 mm. For SiC synthesis we used Si (99%, 325 mesh, Sigma) and C (Norit A supra, surface area (BET), 1700 m^2/g) with 1:1 ratio and 15 wt% PTFE (Sigma-Aldrich powder (free-flowing), 1 μm) and in some cases I applied various amount of aluminum (up to 10 wt%; Alfa Aesar, <325 mesh, 99.8%) to create hexagonal Stacking Faults in the cubic material. The samples were then annealed at 650 °C in air for 10 hours to remove unreacted carbon, then HF:HNO_3:H_2O 1:1:10 (HF: Analar Normapur, 48%; H_2O_2: VWR Normapur, 30%) was used to remove unreacted Si and SiO_2.

Stain etching of SiC: I applied stain etching made under the following condition: HNO_3:HF with a volume ratio of 1:3 was placed along with bulk SiC in PTFE digestion chamber at 150 °C for 2 hours to etch the bulk material. During the reaction porous SiC was formed. After removing the acids and washing the samples, the SiC NP-s were obtained by sonication of the porous SiC macro-crystals in water for 2 hours to remove the porous layer and suspend the NP-s.

Infrared absorption measurements Infrared absorption spectroscopy was used to study the surface properties of SiC NPs Infrared measurements were carried out on drop-drying SiC NPs solutions at the surface of a ZnSe multiple internal reflection crystal and measured in attenuated total internal reflection (ATR) mode.

Equipment: BRUKER Tensor 37 with 4 cm^{-1} resolution and DTGS detector. Spectra were recorded in the 700−4000 cm^{-1} range. The baseline was corrected by an adjusted polynomial function.

UV-VIS and Photoluminescence Measurements Steady state emission spectra were recorded on SiC NPs solution using Xe lamp as a continuous light source by varying the excitation wavelength between 300 nm and 500 nm.

UV-VIS measurements were carried out on Ocean Optics QE6500 spectrometer and Ocean Optics DH-2000-BAL light source.

PL measurements were carried out on these samples using a HORIBA Jobin-Yvon Nanolog FL3-2iHR fluorometer equipped with a 450W Xenon lamp, iHR-3210 grating system, and a R928P photomultiplier tube for the measurement in the ultraviolet and visible range.

For both UV-Vis and PL, quarz quette with 1 cm path length was used.

Electron microscopy I used scanning electron microscopy for visualizing SiC particles and their morphology after synthesis and etching.

Equipment: TESCAN, TESCAN MIRA3

XPS:measurements I used x-ray photoelectron spectroscopy (XPS) measurements to determine the composition of SiC nanoparticles.

Equipment: Twin anode X-ray source (XR4, Thermo Fisher Scientific) and a hemispherical energy analyzer with a 9 channel multi channeltron detector (Phoibos 150 MCD, SPECS). The base pressure of the analysis chamber was around $2 \times 10{-}9$ mbar. Samples were analyzed using a Mg Kα (1253.6 eV) anode, without monochromatization.

Dual beam focused ion beam-scanning electron microscope, and energy-dispersive spectroscopy systems were used to cut through the sample and make the cross section visible for further investigation of the porosity

Equipment: FIB-SEM; (Thermo Fisher FEI Quanta D3) with EDX;(AMETEK Edax Ametek Element detector controlled with APEX software package)

Atomic force microscopy: For size distribution characterization by AFM I used silicon wafer with a roughness of about 0.5 nm. Size distribution was achieved by measuring the height of individual particles.

Equipment: BRUKER, Dimension Icon

We introduced XRD measurements for monitoring the crystal quality. I used the Rietveld-fitting to determine the crystal quality as well as the Stacking Faults of the sample.

Equipment: HUBER G670 Guinier camera, Cu Kα radiation

Electron spin resonance spectroscopy: ESR measurements were performed on a Bruker Elexsys E500 X-band (~ 0.3 T, 9.4−9.8GHz) spectrometer. The sample was under low pressure helium atmosphere to prevent oxidization at elevated temperature.

4. RESULTS AND DISCUSSION

Deepening the understanding of the wet chemical etching of SiC

I examined and upgraded the top-down fabrication method of silicon carbide nanoparticles by constructing an electrochemical theory regarding the mechanism of stain etching of semiconductors. I successfully applied the theory to several semiconductors. By taking advantages of the stain etching being selective to the polytypes I managed to prepare nanoparticles for which size depends on the stacking faults concentration thus enabling more sophisticated size control in the range of 1 nm to 6 nm. Based on the theory I used dithionate compound to modify the etching reagents used for cubic silicon carbide to be able to attack hexagonal polytypes too. As a result I prepared hexagonal silicon carbide nanoparticles.

Stain etching is usually described as an oxidation process. This model struggles to properly explain the SiC polytype selectivity of the applied etching method as the VB of the different polytypes of SiC are rather similar and the main factor of the difference of the bandgap energies comes from the conduction band (CB) position. I proposed and demonstrated that electron injection to the CB, a reduction step, is rather a predominant factor in the initiation of stain etching that facilitates chemical reactions in the solution that creates a strong oxidizing agent that finally leads to hole injection into VB. As a consequence, the interaction of the semiconductor surface with the solution leads to exciton generation without illumination or external bias by this multistep electrochemical process.

By this theory, electron injection is the initiative and most vital step of the process, therefore, the etching process only starts when the conduction band minimum energy lies below the redox potential of a redox couple in the electrolyte.

We named this multistep theory no-photon exciton generation chemistry (NPEGEC).

The VBM of SiC polytypes is considerably higher (more positive) than the redox potential of nitric acid thus the pore formation of cubic SiC polytype should not occur at all by considering only hole injection as a driving force behind the pore formation. However, the CBM values of the polytypes the NPEGEC can explain these phenomenon considering the presence of

the nitrosyl-ion (NO^-) as one of the active agents in stain etching of cubic SiC. NO^- is a very reactive species and the redox potential of NO^-/NO is above the CBM energy of cubic SiC but below the CBM energy of hexagonal polytype, see **Figure 1**. Thus, NO^- is oxidized to neutral NO radical at the cubic SiC surface while it injects an electron into the CB. The resultant NO radicals can inject holes to the VB that oxidizes cubic SiC. Finally, the nucleophile HF is able to dissolve this material.

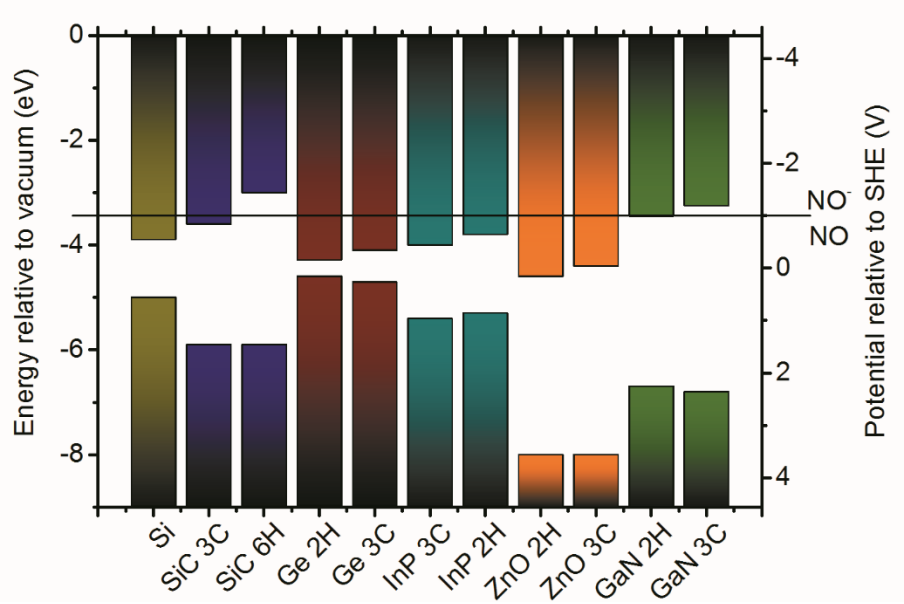

Figure 1.: The redox potential of NO^-/NO versus the band gap of various semiconductors

Chemiluminescence during stain etching

If electrons and holes are simultaneously injected by chemical processes then these generate excitons that may recombine either non-radiatively by phonons or Auger-processes, or radiatively by emitting photons, where the latter can be detected by photodetectors. I observed luminescence during stain etching in dark without applying any external bias. The emission exhibits a maximum at around 610 nm with a shoulder at 535 nm, shown on **Figure 2**.

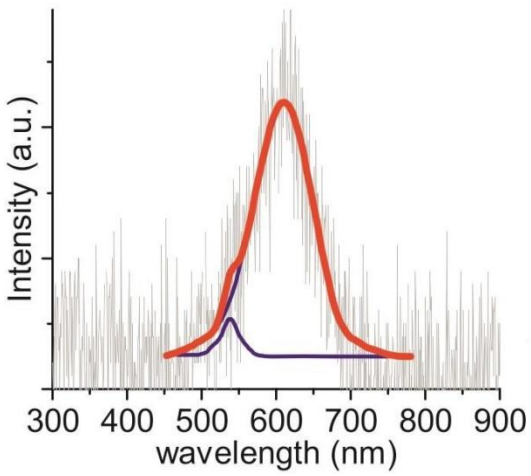

Figure 2.: Chemiluminescence of SiC during stain etching

The role of the Stacking Faults during stain etching

Having established that stain etching is a CB-injection driven process, I concluded that Stacking faults with different CBMs affect the size of the product NPs greatly hexagonal inclusions in cubic SiC act as blocking layers for CB electrons that play a key role in controlling the size of the pore during stain etching. When a semiconductor is immersed in an electrolyte system, band bending takes place to equilibrate the Fermi level. Band bending at the nanoscale is size dependent and as the particle size decreases band bending decreases as well that slows down the electrochemical reaction. Below the size of the exciton Bohr radius band bending blocks the etching. This also means that a certain minimum crystalline size is needed for migration of electrons and holes, in order to develop a depletion layer caused by the band bending effect.

I optimized the synthesis process by using 5 molar % aluminum and 15 wt% of PTFE in order to achieve maximum concentration of stacking faults. Increasing the SF concentration also means that the statistical distance between 2 SF has been reduced.

Size distribution of SiC NPs

A pore wall in the porous layer can be described as interconnected particles. As long as those particles are connected evenly to each other, electron and hole migration is possible and band bending is realized. When the particles are separated or the migration of carriers is hindered then band bending depends only on the size of the separate particles. In this situation, the final particle size during the etching is determined by the exciton Bohr radius. As the migration of the electrons is blocked by the hexagonal inclusions in cubic SiC, the resultant diameter of the SiC NPs should be around twice the exciton Bohr radius which is about 5 nm next to SF. Having the average distance between two SFs reduced, the population of SiC NPs with size close to the exciton Bohr radius increases resulting in a sharper size distribution.

Etching of 6H SiC

As by the NPEGEC I looked for redox couples that could potentially inject an electron to the CB of the 6H-SiC.

The dithionate ($S_2O_6^{2-}$) ion decomposes above 70 °C and various ions and radicals can form including SO_3^{2-} with a reduction potential of -1.36 ± 0.24 V at the $SO_3^{2-}/S_2O_4^{2-}$ redox couple which is sufficient to perform the initative step of the etching by reducing the 6H-SiC.

In the case of the dithionate-hydrofluoric acid treated sample an increased surface porosity and the erosion of the edges can be observed on **Figure 3. (a)-(d)**. It can be suggested that the damage of the edges starts along the crystal dislocations. Repeated etching causes more damaged and porous flats.

Dual beam focused ion beam-scanning electron microscope, and energy-dispersive spectroscopy systems were used to cut through the sample and make the cross section visible for further investigation of the porosity. The cross-section image of the untreated sample shows an undamaged plane and no internal porosity can be observed. On the other hand, in the case of the etched sample, increased porosity has been verified. (**Figure 4. (a)-(d)**)

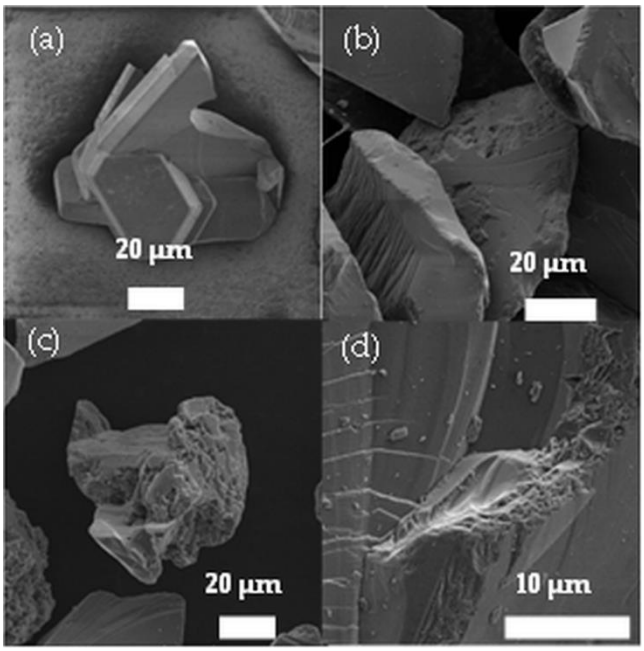

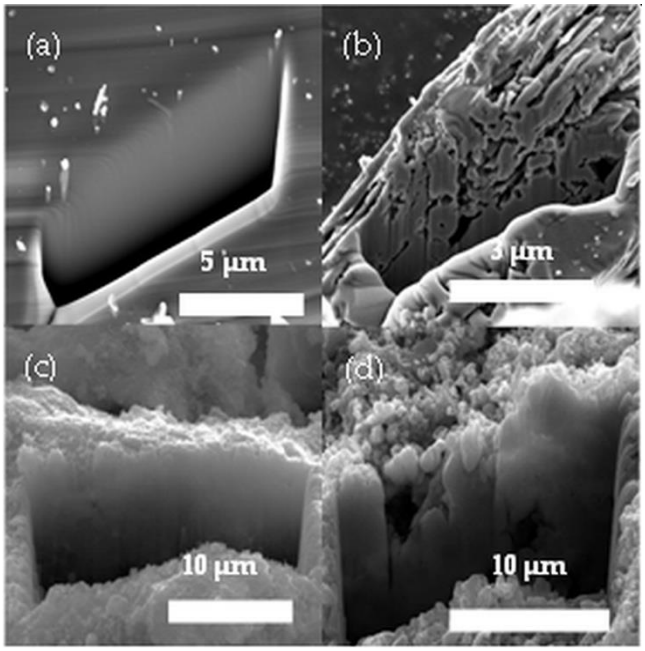

Figure 3. (left): The surface of untreated (a) 6H-SiC that starts eroding during stain etchig (b), followed by sonication (c) and repeated stain etching (d) and **Figure 4. (right):** Cross-section images of (a) untreated 6H¬SiC, (b) etched 6H-SiC, (c) untreated 3C-SiC, (d) etched 3C-SiC.

Creating and identifying 6H NPs by NPEGEC

The product of the etching step was added to approximately 100 ml water and was sonicated for 2 h. During the process, SiC NPs were obtained by mechanically destroying the porous layer. The NPs were separated from the bulk material by centrifuging. The supernatant was once again decanted and pressed through a Pall Acrodisc 32 mm syringe filter with 0.1 µm Supor membrane to eliminate any remaining bulk material.

To identify the composition of the nanoparticles, we applied XPS. Approximately 2 ml of the retentate was dried on a small niobium wafer. First, we identified the adventitious carbon in

the spectrum and shifted the spectrum so the peak position matched the literature data. Then I attempted to identify the silicon bonding as well as the carbon bonding.

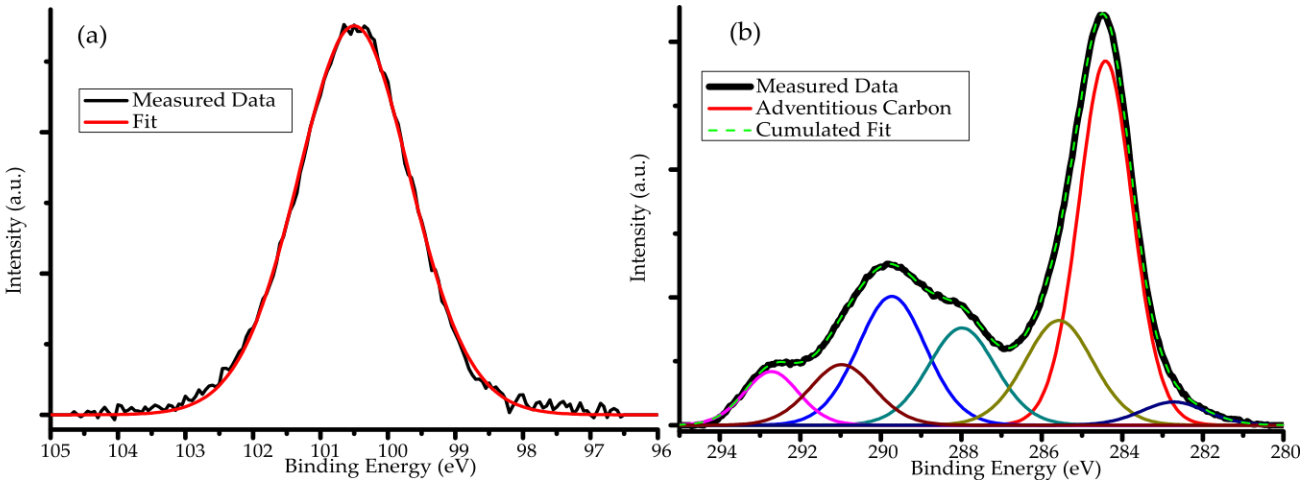

Figure 5.: XPS spectrum and peakfit of **(a)** the Si 2p peak and **(b)** the C 1s peak in the sample

The silicon (Si 2p) peak could be fit by a single gaussian at 100.6 eV (**Figure 5a)**, which is in perfect correlation with the Si–C bonding energy and is a strongly conclusive observation about the composition of the nanoparticle. I also analyzed the carbon peak which turned out to be much more complicated and also less conclusive then the silicon peak but it also suggested the existence of C-Si bonds (**Figure 5b)**.

Size and surface dependent properties of SiC NPs

The most examined semiconductor nanocrystals are well known for being affected by the quantum confinement. While the quantum confinement offers a rather simple explanation for size-dependent optical properties, the Group has demonstrated in 2015 that in the case of case of molecular-sized 3C SiC NPs surface related luminescence is dominant.[15]

Based on my colleagues work, 10 ml aqueous solution of as-prepared SiC NPs (1-4 nm) was used. 0.04 g $NaHCO_3$ and 0.05 g $NaBH_4$ was added to the solution and stirred at room temperature for one hour. In the next step additional 0.05 g $NaBH_4$ was added and the solution was heated up to 80 °C and kept at that temperature for 2 hours. During the reaction the carboxyl groups were reduced and hydroxil terminated particles were formed.

If the emission of SiC NPs is size dependent and there is no surface contribution, peak maxima of the carboxyl terminated and hydroxyl terminated samples should be at the same position, and they should shift with the excitation energy. However, I observed a mixed behavior of the PL peak as a function of the excitation energy.

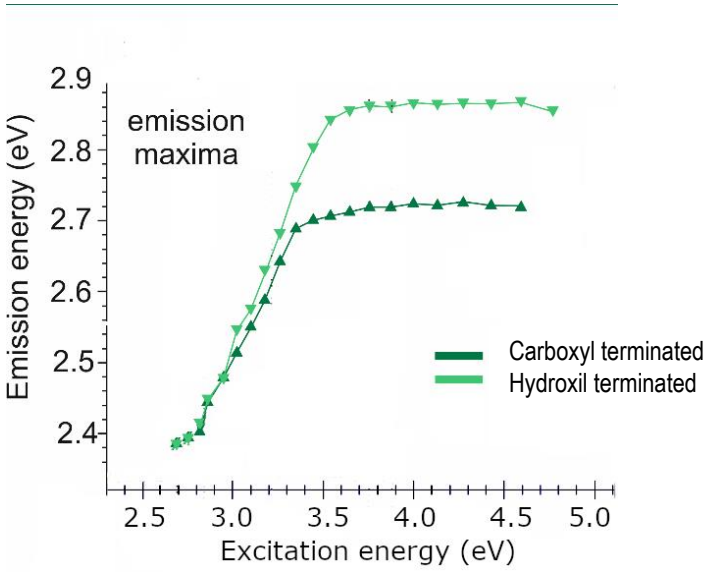

Figure 6.: Emission maxima of SiC NPs versus the excitation energy

At a given range the PL maxima of the carboxyl terminated and the hydroxyl terminated samples were at the same position, shifting with the excitation. Above 2.95 eV excitation, the peak positions of the carboxyl and hydroxyl terminated samples are not identical anymore, see **Figure 6**. The differences between peak positions for carboxyl terminated and hydroxyl terminated samples are increasing between 2.95 eV and 3.3-3.5 eV excitation energies which implies an increasing contribution of surface states in the emission spectra. Ultimately, as the surface contribution becomes dominant over the quantum confinement, the peak positions become static – however they do differ for the samples as the energy level of the surface is also different.

Finding and solving some trivial cases as anchorpoints, I managed to link the recorded optical spectra to the size distribution of the samples, using the effective mass approximation. I observed that the solved equation only fits the datapoints at the larger sizes, while the points at the smaller than 3.5 nm show an increasing deviation from the trendline. This experience ultimately served the conclusion that the quantum confinement is not sufficient alone to describe the particles behavior and is indeed overruled by another effect that shows increasing contribution to the optical properties.

With a modified effective mass approximation equation I managed to fit the observed data sufficiently, and came to the conclusion that the transition point for 3C NPs is at 2.8 nm. Below that point the quantum confinement vanishes and turns into a size independent molecular behavior, and above 3.75 nm the mass approximation is valid.

Improving the nanoparticles for biological applications

As we learned through the microscopic pictures our particles were close to be sphere symmetric and their surface covered by certain functional groups in a homogenous way. This raised the challenge of developing a robust way to substitute only desired groups on the surface. Knowing that *as prepared* NPs are covered with carboxyl groups, and that amino groups usually have very high affiliation to undergo substitutional reactions I decided to attempt to create a

peptide bond between the carboxylated NPs and an amino-terminated reactant. I also decided that the aminotermination should be immobilized on a solid phase surface so the steric hindrance would effectively prevent the reaction of all the functional groups on the NPs surface.

For starting material I decided to use a low surface roughness silicon wafer (2.5 inches, (100) surface). This surface was oxidized with a 1:1 mixture of 96% sulphuric acid and 30% hydrogen-peroxide. During the reaction a uniform, oxidized layer on the wafer was formed. This was further functionalized with 3-aminopropyltriethoxysilane (APTES; Aldrich, 99%) creating an immobilized aminoterminated surface on the siliconwafer.[16] For the peptide coupling with the NPs the chosen reactant was N,N′-Dicyclohexylcarbodiimide (DCC; VWR, 99%).

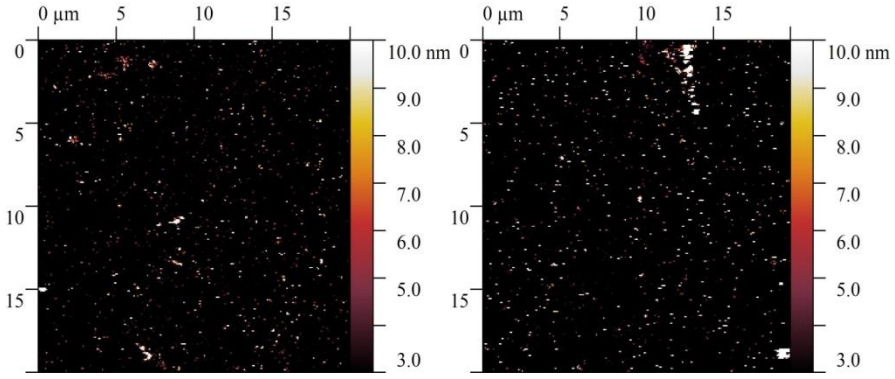

Figure 7.: Immobilized SiC NPs on Si wafer before and after surface cleansing

After the reaction the surface was cleaned by an excessive amount of deionized water and was briefly sonicated as well in order to remove the chemically not bound particles from the surface, shown on **Figure 7**. On the other hand, removing particles with kinetic energy did not seem to be highly selective so it was high priority not to overuse the cleaning methods.

These initiative experiments suggest that the immobilization of the SiC NPs via peptide bonding is possible, albeit there is still room for improvement when it comes to the selectivity or the yield of this method. This could potentially serve as an anchor point for peptide synthesis using SiC NPs as biomarker.

The examination of interaction between SiC NPs and a model protein

As initial step of examining the SiC NP – Protein interactions we decided to use Bovine Serum Albumine (BSA) for testing. Serum albumins are the most abundant proteins in the blood, and their major physiological role is to carry various ligands to their respective target organs.

To examine the interaction between the BSA and the SiC NP-s I measured the absorbtion and the PL spectra of the solutions on their own as well as of the mixture of the two including fluorescence lifetime measurements as well. The fluorescence intensity decreases with increasing SiC NP content of the samples, which indicates fluorescence quenching by the NPs (**Figure 8.)**.

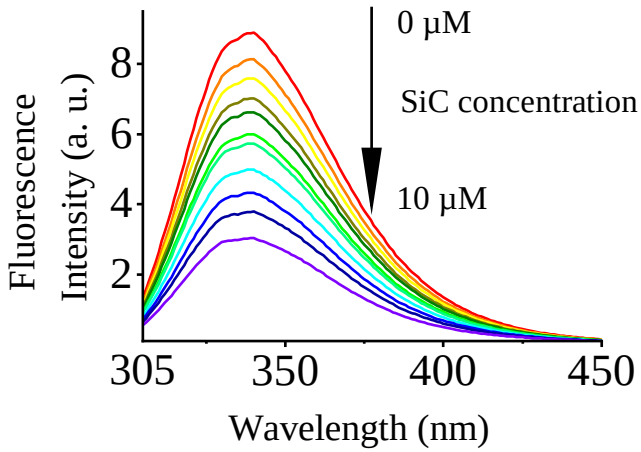

Figure 8.: The PL spectrum of BSA in increasing presence of SiC NPs.

To further examine the nature of the quenching I created the Stern-Volmer representation of the measured spectra. The Stern–Volmer plot of the luminescence quenching constructed from the luminescence intensity shows complex or mixed interactions; For small SiC NPs, there is a positive deviation from the linearity for the lifetime, too.

The curve of I_0/I shows higher values than τ_0/τ on the Stern-Volmer plot (**Figure 9.)** which is often explained by both static and dynamic quenching occurring during this process. Similarly, the upward-curving nature of the Stern-Volmer trend reveals the presence of a complex fluorescence-quenching mechanism.

I investigated a possible energy transfer between the BSA and the nanoparticles. As there is a large spectral overlap between BSA emission and SiC NPs absorption (**Figure 10.)**, Hiba! A hivatkozási forrás nem található.the possibility of Förster resonance energy transfer (FRET) quenching seemed to be an ideal candidate to describe the observed phenomenon.

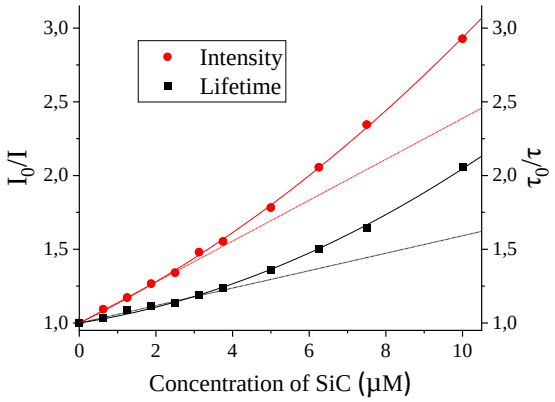

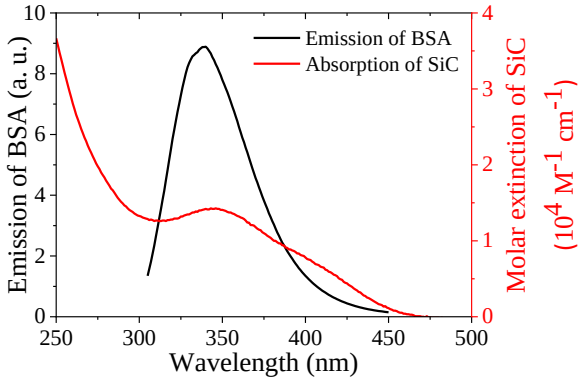

Figure 9.(left): The Stern-Volmer plot of the BSA-SiC system and
Figure 10.(right): the optical emission of the BSA overlaps with the absorbtion spectrum of the SiC NPs

FRET occurs when the donor fluorophore absorbs a photon, and the excitation energy is transferred to an acceptor molecule close to the donor. FRET efficiency highly depends on the distance between the donor and acceptor molecules. In most cases, this distance is fixed. In this system the donor–acceptor distance is constantly changing in time and can only be described by an average distance which depends on the concentration of the NPs. From Förster's theory, the Förster radius (R_0) can be calculated. The applied parameter values were $\kappa^2 = 2/3$, n = 1.34 and $\Phi_D = 0.15$ based on literature data. These parameters resulted $R_0 = 2.83$ nm which was comparable to the size of the NPs and also generally speaking acceptable result for a FRET distance.

Besides FRET, I tested hydrogen bond-mediated complex formation and the quenching sphere of action model as possible interactions between the NP and the protein and finally concluded that SiC NPs and BSA interact in an inhibited diffusion manner and such a mechanism results in a complex quenching reaction, which shows second-order dynamic and static quenching without causing permanent changes to the protein structure. In addition, I identified the reaction partner of the NPs where the energy transfer occurs to be the Trp212 and the best explanation for the quenching method is FRET. The lack of evidence for BSA denaturation in the presence of SiC, and the absence of a strong complex or protein corona formation imply in vivo biocompatibility for SiC below 10 nm as well. There is hope that a functionalized nanoparticle will keep its designed properties, including point defects induced optical properties in complex biological media.

Generating point defects in a controlled manner

As it was mentioned before, bulk SiC may contain various types of point defects that do modify the properties of the material, e.g. they may be magneto-optically active or may act as a carrier trap. The introduction of the point defects may occur *in situ* during the reaction but also can happen after the synthesis has been completed. As the vast majority of point defects can be classified as an atomic-level dislocation one usually uses some sort of radiation with high energy in order to remove or relocate an atom inside the crystal. The most typical particles to bombard the atoms in the lattice are either ions or electrons or neutrons. While these bombardments are not exactly selective to the point defects, those defects have differentiated thermal stability and thus can be selectively removed by thermal annealing of the sample.

During the experiment we used combustion synthesis to create SiC with high amount of stacking faults using aluminum precursor and used neutron irradiation (10^{18} cm^{-2}) to introduce point defects to the bulk sample. The sample was consecutively annealed to 800 °C and in each step it was measured by ESR to monitor the changes occurring to the point defects (**Figure 11.**).

Based on the portrayed graphs it can be concluded that the neutron irradiation generated new, ESR active point defects that were slowly eliminated upon annealing without actually returning to the original state of the material. In order to identify the present point defects in the ESR spectrum I decided to fit the spectra using the Easyspin module of the Matlab program.

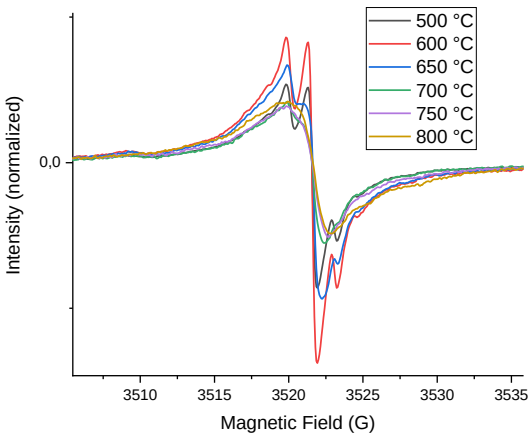

Figure 11.: Transformation of the ESR spectrum during annealing

The results indicate that the spectra contain a mixture of two or three different point defects, namely silicon vacancy (V_{Si}), carbon vacancy (V_C), and carbon antisite-vacancy pair ($C_{Si}V_C$). In a reduced concentration the initial defects at 500°C are still present at 800°C and a new type of defect which was identified as $C_{Si}V_C$ was formed during the annealing, shown on **Figure 12** and **Table 1.** This result is can be explained by the well-known transition of V_{Si} into $C_{Si}V_C$. In all of my fittings only these three type of defects were found. I created a comparative table of the relative concentration of these point defects that demonstrates the transformation of V_{Si} into $C_{Si}V_C$ versus the annealing temperature.

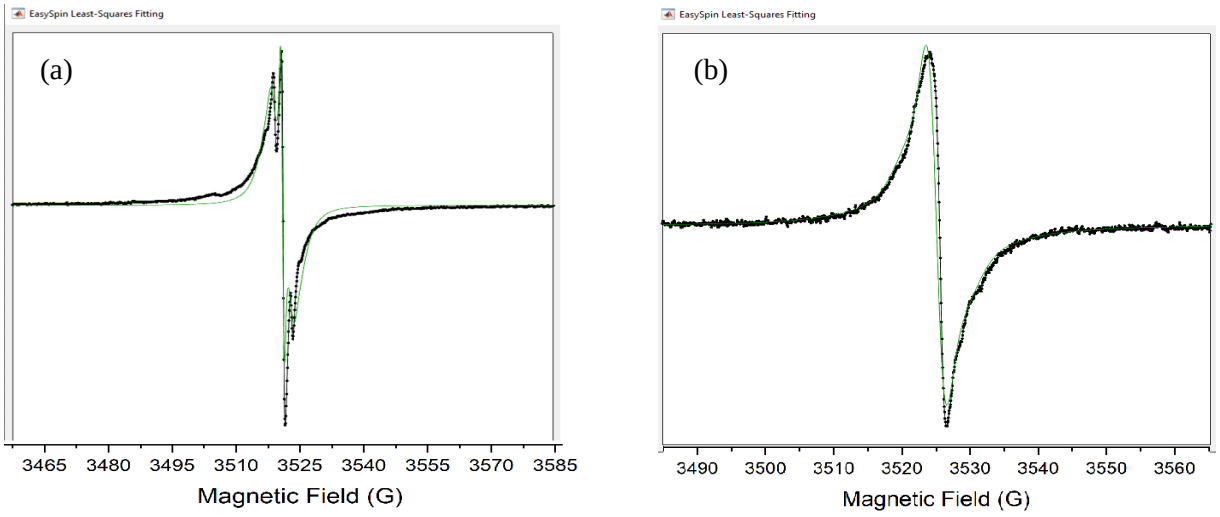

Figure 12.: Easyspin fitting of the 500°C annealed sample (a) and the 800°C annealed sample (b).

The fitting suggests that throughout the steps of annealing the relative amount of Vc starts to decrease and therefore the relative amount of V_{Si} starts to increase. This trend continues to be present until 700 °C when a drastic shift is observed in the spectrum as well as in the fitting. The monotonous decrease of the Vc seems to be obvious and in harmony with the expectations. At

700 °C a new presence, the $C_{Si}V_C$ is confirmed and it is indicated that it is formed at the expense of the V_{Si} in the sample. With a low level of uncertainty it can be concluded that the neutron irradiation induced mostly the two basic types of point defects in our 3C-SiC sample. This experiment gives us an improved way to create 3C-SiC samples with selectively enriched point defects using irradiation and annealing. These measurements did not confirm the presence of divacancy in 3C-SiC but it demonstrated the presence of V_{Si} which is a good candidate for sensing.

Temperature	V_{Si}	V_C	$C_{Si}V_C$
500 °C	64.0%	36.0%	-
600°C	77.0%	23.0%	-
650°C	81.0%	19.0%	-
700°C	22.3%	20.4%	57.3%
750°C	15.7%	17.3%	67.0%
800°C	14.2%	17.2%	68.5%

Table 1.: Quantitative analysis of point defects during the annealing process

5. OUTLOOK AND FUTURE APPLICATIONS

At current time SiC NP <100 nm particles are available on the market containing primarily beta phase SiC (Sigma).

The surface modification by coupling agents has been remained and remains to be intensively studied for various purposes by other groups throughout my research years.[17,18,19]

The past decade of the quantum dots in clinical research has been dominated by materials that pose high threat of *in vivo* toxicity and methods of mitigating the risks of application. [20]

Similarly to the cubic SiC, the two closely-related material, hexagonal SiC and diamond are also being examined excessively for potential quantum technology applications based on their defects and paramagnetic centers.[21,22]

While SiC is at some sort of tempo disadvantage compared to diamond for the reason of being discovered later, its outstanding properties and the demonstrated similarities with the nanodiamond-based materials show great promise for reaching or even exceeding the significance of its predecessor in the research and development field.

6. THESIS

The main conclusions of my PhD work are summarized in the following thesis points. The related results were published in 4 different articles referred as T1, T2, T3 and T4.

1) I examined and upgraded the top-down fabrication method of silicon carbide nanoparticles (T1)

    a) I constructed an electrochemical theory regarding the mechanism of stain etching of semiconductors, stating that electron injection to the conduction band, a reduction step, is the most vital step in the the initiation of stain etching. Therefore, the etching process only starts when the conduction band minimum energy lies below the redox potential of a redox couple in the electrolyte, and hole injection into the valence band only occurs at a later stages. I succesfully applied the theory to several semiconductors. (T1)
    b) By using aluminium and poly-tetrafluoroethylen as additional reagents I prepared such bulk cubic silicon carbide that contained respectively 15% of hexagonal inclusion also known as stacking faults in a controlled manner. By taking advantages of the stain etching being selective to the polytypes I managed to prepare nanoparticles for which size depends on the stacking faults concentration thus enabling more sophisticated size control in the range of 1 nm to 6 nm. (T1)
    c) Based on the theory I modified the etching reagents used for cubic silicon carbide to be able to attack hexagonal polytypes too. I chose to use dithionate compound as its redox potential suited better the conduction band minimum energy of the 6H-SiC. As a result I prepared hexagonal silicon carbide nanoparticles with the size of under 50 nanometers in both the permeate and the retentate with the mode around 3 nm and 5 nm, respectively. The particles luminesce in the visible and show quantum confinement. (T2)

2) I succesfully separated 1 nm to 6 nm nanoparticles into two fractions containing mostly particles of 1 nm to 3 nm and 4 nm to 6 nm.

    a) I prepared samples with different size distribution and surface and demonstrated that silicon carbide nanoparticles have size dependent optical properties. I constructed a mathematical theory and showed that for ultrasmall nanoparticles the surface states dominate over quantum confinement regarding the contribution to the optical properties. I also identified that the transition point between the two regions of the phenomena is estimated to be at around 2.85 nm. (T3)

3) I participated on the surface modification of silicon carbide nanoparticles improving their uses in biological applications. (T3, T4)

    a) Using IR, PL and UV-Vis as optical analytical measurements I identified fluorescence quenching between bovine serum albumin and silicon carbide nanoparticles as a complex phenomenon that can be described as a mixture of

static and dinamic quenching. I located the site of the energy transfer at the tryptophan group of the BSA. (T4)

4) I succesfully created point defects in controlled manner that enhance the material for possible quantum technological application.

   a) I demonstrated a that irradiation is a viable option for introducing point defects to the material, significantly changing its ESR spectrum. I used computing methods to characterize those point defects and identified them to be silicon vacancy and carbon vacancy. I applied thermal annealing to manipulate the concentration of them, resulting in a slightly selective elimination of the carbon vacancy then at 700 °C triggering the silicon vacancies trasformation into an antisite-vacancy complex defect.

Publications supporting the Thesis points

T1: David Beke, Gyula Károlyházy, Zsolt Czigány, Gábor Bortel, Katalin Kamarás & Adam Gali, Harnessing no-photon exciton generation chemistry to engineer semiconductor nanostructures, *Scientific Reports* **7** 10599 (2017).
https://doi.org/10.1038/s41598-017-10751-x **IF.:4.61** **Cit.: 10**

T2: Gyula Károlyházy, Dávid Beke, Dóra Zalka, Sándor Lenk, Olga Krafcsik, Katalin Kamarás and Ádám Gali, Novel Method for Electroless Etching of 6H-SiC, *Nanomaterials* **10** 538 (2020).
https://doi.org/10.3390/nano10030538 **IF. 5.076:** **Cit.: 3**

T3: David Beke, Anna Fučiková, Tibor Z. Jánosi, Gyula Károlyházy, Bálint Somogyi, Sándor Lenk, Olga Krafcsik, Zsolt Czigány, János Erostyák, Katalin Kamarás, Jan Valenta, and Adam Gali, Direct Observation of Transition from Solid-State to Molecular-Like Optical Properties in Ultrasmall Silicon Carbide Nanoparticles, *The Journal of Chemical Physics C* **122** 26713-26721 (2018).
https://doi.org/10.1021/acs.jpcc.8b07826 **IF.:4.309** **Cit.:5**

T4: Gabriella Dravecz, Tibor Z. Jánosi, Dávid Beke, Dániel Á. Major, Gyula Károlyházy, János Erostyák, Katalin Kamarás and Ádám Gali, Identification of the binding site between bovine serum albumin and ultrasmall SiC fluorescent biomarkers, *Physical Chemistry Chemical Physics* **20** 13419-13429 (2018).
https://doi.org/10.1039/C8CP02144A **IF.:3.567** **Cit.:9**

Further publications

Zsolt Szekrényes, Bálint Somogyi, Dávid Beke, Gyula Károlyházy, István Balogh, Katalin Kamarás, and Adam Gali, Chemical Transformation of Carboxyl Groups on the Surface of Silicon Carbide Quantum Dots, The Journal of Physical Chemistry C **118** 19995-20001 (2014).
DOI:10.1021/jp5053024 **IF.: 7.458** **Cit.:9**

Dávid Beke, Jan Valenta, Gyula Károlyházy, Sándor Lenk, Zsolt Czigány, Bence Gábor Márkus, Katalin Kamarás, Ferenc Simon, and Adam Gali, Room-Temperature Defect Qubits in Ultrasmall Nanocrystals The Journal of Physical Chemistry Letters **11** 1675-1681 (2020) https://doi.org/10.1021/acs.jpclett.0c00052 **IF.: 6.475 Cit.:11**

Conference presentations

„Ponthibák szabályozott előállítása szilícium-karbidban" Poster presentation at the ELFT conference (2016)

„Fém-adalékolt SiC kristályok előállítása és vizsgálata" Oral presentation at the ELFT summer school (2014)

„Preparation of Doped Silicon Carbide Quantum Dots" Poster presentation at SIWAN6 conference (2014)

7. REFERENCES

1. Vonesch, C., Aguet, F., Vonesch, J.-L. & Unser, M. The colored revolution of bioimaging. *IEEE Signal Process. Mag.* **23,** 20–31 (2006).
2. H. Soo Choi, W. Liu, P. Misra, E. Tanaka, J. P. Zimmer, B. Itty Ipe, M. G. B. J. V. F. Renal clearence of quantum dots. *Nat. Biotechnol.* **25,** 1165–1170 (2007).
3. Choi, H. S. *et al.* Design considerations for tumour-targeted nanoparticles. *Nat. Nanotechnol.* **5,** 42–47 (2010).
4. Michalet, X. Quantum Dots for Live Cells, in Vivo Imaging, and Diagnostics. *Science (80-.).* **307,** 538–544 (2005).
5. Medintz, I. L., Uyeda, H. T., Goldman, E. R. & Mattoussi, H. Quantum dot bioconjugates for imaging, labelling and sensing. *Nat. Mater.* **4,** 435–446 (2005).
6. Shao, L., Gao, Y. & Yan, F. Semiconductor Quantum Dots for Biomedicial Applications. *Sensors* **11,** 11736–11751 (2011).
7. Smith, A. M., Mancini, M. C. & Nie, S. Bioimaging: Second window for in vivo imaging. *Nat. Nanotechnol.* **4,** 710–711 (2009).
8. Lim, Y. T. *et al.* Selection of Quantum Dot Wavelengths for Biomedical Assays and Imaging. *Mol. Imaging* **2,** 50–64 (2003).
9. Abderrazak, H. & Hadj Hmi, E. S. B. in *Properties and Applications of Silicon Carbide* 361–389 (InTech, 2011). doi:10.5772/15736
10. Sörman, E. *et al.* Silicon vacancy related defect in 4H and 6H SiC. *Phys. Rev. B* **61,** 2613–2620 (2000).
11. Torpo, L., Marlo, M., Staab, T. E. M. & Nieminen, R. M. Comprehensive ab initio study of properties of monovacancies and antisites in 4H-SiC. *J. Phys. Condens. Matter* **13,** 6203–6231 (2001).
12. Merrifield, R. B. Solid Phase Peptide Synthesis. I. The Synthesis of a Tetrapeptide. *J. Am. Chem. Soc.* **85,** 2149–2154 (1963).

13. Kharazian, B., Hadipour, N. L. & Ejtehadi, M. R. Understanding the nanoparticle–protein corona complexes using computational and experimental methods. *Int. J. Biochem. Cell Biol.* **75,** 162–174 (2016).
14. Bai, X., Wang, J., Mu, Q. & Su, G. In vivo Protein Corona Formation: Characterizations, Effects on Engineered Nanoparticles' Biobehaviors, and Applications. *Front. Bioeng. Biotechnol.* **9,** 1–16 (2021).
15. Beke, D., Szekrényes, Z., Czigány, Z., Kamarás, K. & Gali, Á. Dominant luminescence is not due to quantum confinement in molecular-sized silicon carbide nanocrystals. *Nanoscale* **7,** 10982–10988 (2015).
16. Ruiz-Cañas, M. C., Corredor, L. M., Quintero, H. I., Manrique, E. & Romero Bohórquez, A. R. Morphological and Structural Properties of Amino-Functionalized Fumed Nanosilica and Its Comparison with Nanoparticles Obtained by Modified Stöber Method. *Molecules* **25,** 2868 (2020).
17. Shang, X., Zhu, Y. & Li, Z. Surface modification of silicon carbide with silane coupling agent and hexadecyl iodiele. *Appl. Surf. Sci.* **394,** 169–177 (2017).
18. Utara, S., Jantachum, P. & Sukkaneewat, B. Effect of surface modification of silicon carbide nanoparticles on the properties of nanocomposites based on epoxidized natural rubber/natural rubber blends. *J. Appl. Polym. Sci.* **134,** 45289 (2017).
19. Bělinová, T. *et al.* Immunomodulatory Potential of Differently-Terminated Ultra-Small Silicon Carbide Nanoparticles. *Nanomaterials* **10,** 573 (2020).
20. Wagner, A. M., Knipe, J. M., Orive, G. & Peppas, N. A. Quantum dots in biomedical applications. *Acta Biomater.* **94,** 44–63 (2019).
21. Csóré, A., Son, N. T. & Gali, A. Towards identification of silicon vacancy-related electron paramagnetic resonance centers in4H -SiC. *Phys. Rev. B* **104,** 035207 (2021).
22. Gulka, M. *et al.* Room-temperature control and electrical readout of individual nitrogen-vacancy nuclear spins. *Nat. Commun.* **12,** 4421 (2021).